

# Non-Prehensile Tool-Object Manipulation by Integrating LLM-Based Planning and Manoeuvrability-Driven Controls

<sup>1</sup>Hoi-Yin Lee, <sup>2</sup>Peng Zhou, <sup>3</sup>Anqing Duan, <sup>4</sup>Wanyu Ma, <sup>5</sup>Chenguang Yang, <sup>1,\*</sup>David Navarro-Alarcon

<sup>1</sup>The Hong Kong Polytechnic University, Hong Kong.

<sup>2</sup>The Great Bay University, China

<sup>3</sup>Mohamed Bin Zayed University of Artificial Intelligence, UAE

<sup>4</sup>The Chinese University of Hong Kong, Hong Kong

<sup>5</sup>University of Liverpool, United Kingdom

\*Corresponding author.

Keywords: *Tool manipulation; Task allocation; Affordance modelling; Task and motion planning; Robotics.*

The ability to wield tools was once considered exclusive to human intelligence, but it's now known that many other animals, like crows, possess this capability. Yet, robotic systems still fall short of matching biological dexterity. In this paper, we investigate the use of Large Language Models (LLMs), tool affordances, and object manoeuvrability for non-prehensile tool-based manipulation tasks. Our novel method leverages LLMs based on scene information and natural language instructions to enable symbolic task planning for tool-object manipulation. This approach allows the system to convert the human language sentence into a sequence of feasible motion functions. We have developed a novel manoeuvrability-driven controller using a new tool affordance model derived from visual feedback. This controller helps guide the robot's tool utilization and manipulation actions, even within confined areas, using a stepping incremental approach. The proposed methodology is evaluated with experiments to prove its effectiveness under various manipulation scenarios.

## 1 Introduction

Being able to use tools is a widely recognised indicator of intelligence across species [1,2]. Humans, for instance, have demonstrated mastery of tool use for over two million years [3]. The ability to use tools is invaluable as it extends an organism's reach and enhances its capacity to interact with objects and the environment [1]. Being able to understand the geometric-mechanical relations between the tools-objects-environments allows certain species (e.g., apes and crows [4]) to reach food in narrow constrained spaces. The same principles of physical augmentation and its associated non-prehensile manipulation capabilities also apply to robotic systems [5]. For example, by instrumenting them with different types of end-effectors, robots can (in principle) dexterously interact (e.g., push and flip) with objects of various shapes and masses akin to its biological counterpart [6–8]. However, developing this type of manipulation skill is still an open research problem. The goal of this paper is to develop a methodology to effectively transport objects through non-prehensile tool manipulation actions.



Figure 1: Tool-Object manipulation in a dual-arm robotics system with environmental constraints using the non-prehensile approach.

### 1.1 Related Works

Effective tool utilisation by a robot involves primarily two aspects: (1) task planning and (2) tool movement [9–11]. Task planning is typically regarded as a cognitive high-level process in robotics, mainly used for environmental reasoning, task decomposition, allocation of action sequences, etc. [12]. Task can be decomposed with the integration of learning-based approaches, particularly through the use of reinforcement learning techniques to optimize task planning [13–15]. Studies have also highlighted the effectiveness of rule-based planning methods, which incorporate predefined heuristics and logical rules to enhance the efficiency of task decomposition in structured environments [16–19]. While rule-based planning is effective for well-defined problems, it can struggle with complex, dynamic environments where the number of rules may become unmanageable. However, recent trends have been pushing towards the use of LLMs to leverage the domain knowledge for semantically decomposing and planning the execution of manipulation tasks [20–25]. Some examples of this direction include [21,22], which developed an environmental feedback-based system for context-aware improvement planning. Leveraging the generative capabilities of LLMs, motion sequences can be generated for robots as demonstrated in [23,26,27]. The combination of traditional motion planners with LLMs has been explored in [20,28,29]. Domain knowledge can be integrated with LLMs to generate a list of motions for navigating a robot in an apartment, as demonstrated in [25]. However, the focus primarily remains on independent motions. Motivated by [25], we further consider the dependent motion among arms and tools.

Transitioning from the critical role of task planning, it is evident that effective tool use is inherently tied to understanding the relationship between tools and objects. Indeed, the success of a given tool-object manipulation task largely depends on the appropriate selection of the tool, which necessitates a nuanced comprehension of how tools interact with

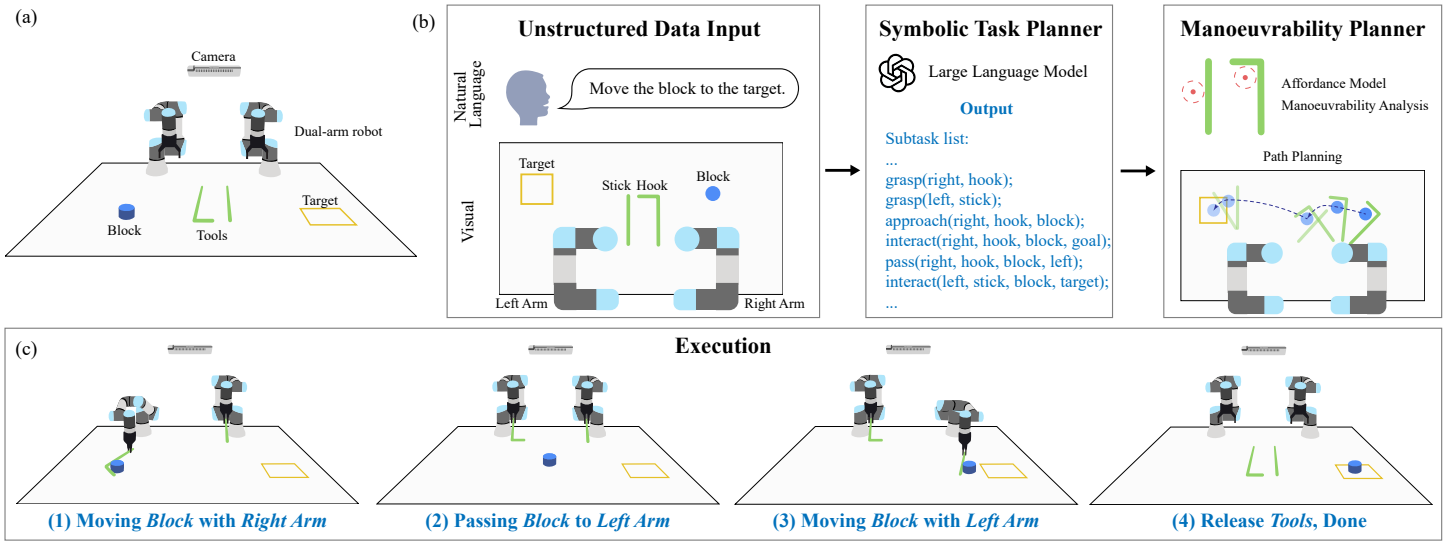


Figure 2: (a) The task environment includes a camera for real-time top-view capturing, a dual-arm robot, tool(s), and a blue manipulandum to be manipulated to the target location. (b) The architecture of our system: Unstructured data input is converted to a subtask list in the symbolic task planner with an LLM, a manoeuvrability-driven planner to compute the tool’s manoeuvrability and generate an affordance-oriented motion and path. (c) Execution process of the result given by the system: dual-arm robots take turns pushing the blue manipulandum from one side to another via collaboration.

various objects in their environment [30]. For example, robots can identify the tool type, potential uses, and contact approaches based on the tool’s geometry, see e.g., [2, 9]. In [31], tool features are learned through observation of the task’s effects and experimental validation of feature hypotheses. Affordance models are a common technique used for tool feature selection [32–34] and tool classification [34–36]. The relation between tool actions and its effects on objects is explored in [36, 37], where robots acquire affordance knowledge through predefined actions (e.g., pull, push, rotate). Recently, researchers have also explored the use of LLM in accelerating affordance learning in tool manipulation [2]. Some works have studied tool-based manipulation under constraints and from demonstrations [38, 39]. Non-prehensile object manipulation strategies have been used in [40, 41].

Building on this foundation of understanding tool-object interactions, it is important to highlight that, despite the advancements in robotic tool use, collaborative tool-based object manipulation by dual-arm systems based on non-prehensile actions remains an underexplored problem. Notably, the challenge of applying incremental control on the stepping motion of the tool within a confined area has not been well-addressed by previous studies [2, 9, 30–39]. Furthermore, most studies have primarily focused on task decomposition for simple object manipulation using LLMs, with tool manipulation being rarely addressed. Dual-arm collaborative manipulation utilizing non-prehensile tools represents a promising area for further exploration. In other words, the integration of LLMs in tool-object manipulation with dual-arm robots remains underexplored. This specific challenge continues to present an open opportunity in the field.

## 1.2 Contributions

To address this research gap, in this work, we propose a novel LLM-based manoeuvrability-driven method with the

following original contributions: (1) We develop an effective model to represent the geometric-mechanical relations and manoeuvrability of tools and objects; (2) We propose a non-prehensile strategy to manoeuvre objects under different constraints with tools; (3) We evaluate the performance of the proposed methodology with real-world experiments on a dual-arm robotic system. Our work uniquely integrates LLMs to enhance tool-object interactions, enabling robots to interpret and execute complex non-prehensile manipulation tasks through natural language instructions. This integration allows for dynamic adaptation to various situations and fosters intuitive human-robot collaboration, significantly improving the effectiveness of dual-arm tool-object manipulation.

The rest of the manuscript is organised as follows: Sec. 2 presents the methodology, Sec. 3 presents the results, Sec. 4 gives final conclusions.

## 2 Methodology

### 2.1 Problem Formulation

Consider a dual-arm robotic system using a tool to manipulate a block at a far distance (see Fig. 1). Given the input is a free-form language task  $\mathbf{L}$  (e.g., “move the block to Point B”), we apply a high-level symbolic planner (i.e., an LLM) to decompose the task into multiple subtasks  $\mathbf{l}_i$ ,  $\mathbf{L} = \{\mathbf{l}_1, \mathbf{l}_2, \dots\}$  where  $\mathbf{L}$  contains a list of pre-defined motion functions  $\mathbf{l}_i$ .

We define a *tool* as a manipulable object that is graspable by a robot, a *manipulandum* [9] as an object (e.g. a block) that is manipulated via a tool, and a *wall* as a static non-manipulable object. Tool use by robots is challenging as the tools can have various shapes, the environment can be dynamic, and the contact between the tool and the manipulandum may be hard to maintain in a long-horizon task. In this study, we focus on using the side part of a tool to interact with the *manipulandum*. Depending on the geometric

features of a tool and a wall, the available affordance for manoeuvring a manipulandum may be different. Affordance here refers to the available action-effects offered by the tool or the environment. In this work, we classify affordance into two types: active and passive. Active affordance is given from a manipulable object, i.e. a tool, and it is directly related to the manoeuvrability when driving a manipulandum. Passive affordance is given from a static non-manipulable object.

To derive our methodology, the following setup assumptions are made: (1) The manipulation motion is planar, (2) the size of the manipulandum is not larger than any one of the segments of the tool, and (3) the manipulandum has a simple, regular geometric shape, such as circular or hexagonal. Throughout this paper, “tool-based object manipulation” is denoted as TOM, and “tool-based object manipulation under environmental constraints” is denoted as TOME. Also,  $\mathbf{p}^\circ$  represents the 2D pose of an object  $\circ$ . The complete architecture of our method is depicted in Fig. 2.

## 2.2 LLM-Based High-Level Symbolic Task Planner

To obtain a valid task decomposition for a long-horizon task, the system needs to understand the requirements and generate an executable subtask list. We develop a symbolic task planner that takes natural language instructions with scene descriptions as input, and outputs a list of high-level subtasks. The list involves the tool selection/sharing between two arms, the sequence to manipulate the tool with the manipulandum, and the interaction between the two arms. The model is fine-tuned using approximately 20,000 example data lists, specifically tailored for our non-prehensile tool object manipulation scenario. During the fine-tuning stage, we utilized a program to create 20,000 distinct environmental setups by randomly varying the poses of the robot, tool, block, and target within a finite combination space. This approach allows task decomposition to be framed as a classification problem, enabling the LLM to effectively correlate each setup with a specific list of motion functions, thereby enhancing its ability to predict expected outcomes based on prompt patterns rather than producing hallucinations.

The system interprets the provided high-level task  $\mathbf{L}$ , which can have a structure like “Please move the blue block to the right-hand side”, “Can you push the block to the target?”, etc. Visual information of the scene is grounded to the system from the observation data  $\mathbf{o}$ , where  $\mathbf{o}$  is composed of a series of data points, such as the pose of the block (manipulandum), tools, robots, and walls. The system embeds the environmental information with the task instruction to produce a desired configuration requirement, denoted as  $\{\mathbf{p}^{\text{obj}}, \mathbf{p}^{\text{target}}, \dots\} \leftarrow f(\mathbf{L}, \mathbf{o})$  where  $f(\mathbf{L}, \mathbf{o})$  is the embedded result.

The LLM interprets the output of  $f(\mathbf{L}, \mathbf{o})$  to generate a subtask list  $\{\mathbf{l}_1, \mathbf{l}_2, \dots\} \leftarrow f_{\text{llm}}(f(\mathbf{L}, \mathbf{o}))$  where  $\mathbf{l}_i$  is a subtask describing the manipulation phase of each robot [42] and is corresponding to a high-level robot motion function. The motion functions are designed to be simple and specify a short-term goal of the concerned object (these functions omit low-level motion commands). For simplicity, here we use  $m$  to represent manipulandum in the following function definitions. We use `grasp(arm, tool)` for grasping a *tool*

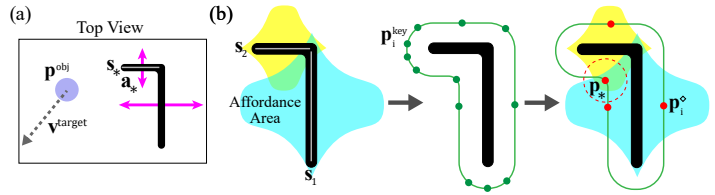


Figure 3: (a) Affordance vectors are shown in pink arrows. Grey arrow is  $\mathbf{v}^{\text{target}}$  and the desired affordance vector is denoted as  $\mathbf{a}_*$ . (b) shows the manoeuvrability analysis flowchart: affordance area is visualised with the Gaussian function in yellow and blue; expand and downsample the tool’s shape to get key points  $\mathbf{P}^{\text{key}}$  (green colour dots); combine the affordance area with the key points  $\mathbf{P}^{\text{key}}$  to get the non-redundant points  $\mathbf{P}^\circ$  (red dots), and combine the affordance  $\mathbf{a}_*$  found in (a) to obtain the position for the manipulandum to be at with the tool (labelled as  $\mathbf{p}_*$  with a red dot) and the highest manoeuvrability region is shown with a dashed red circle.

with the robot *arm*; `approach(arm, tool, m)` for approaching the location of  $m$  with *tool* using *arm*; `interact(arm, tool, m, goal)` for moving  $m$  to the *goal* location with the *tool*; `stepping(arm, tool, m)` for moving  $m$  out from the bounded area with the *tool* of the *arm* through contact pulsing motions; `pass(arm1, tool, m, arm2)` for passing  $m$  to another arm’s workspace; `release(arm, tool)` for releasing the *tool* back to its original place with the *arm*.

A sample motion task with a dual-arm robot is given as: `{pass(right, hook, block, left); approach(left, stick, block); interact(left, stick, block, target); ...}`  $\leftarrow f_{\text{llm}}(f(\mathbf{L}, \mathbf{o}))$  where both arms take turns manipulating the block. The right arm passes the block to the left by pushing it to an area where both arms can reach it. The left arm approaches the block with a stick and manipulates the block to the target. To this end, the symbolic task planner converts the unstructured data to a series of motion functions, including robot motion, tool planning, manipulation sequence, and collaboration.

## 2.3 Visual Affordance Model

Tools can have various shapes and complex structures. In this paper, we focus on the following tool geometries: a stick, an L-shaped hook, and a Y-shaped hook. Affordances are related to the geometric features of a tool [43]. To analyse the possible affordances, we divide the tool into smaller segments (i.e. a line), and denote them as  $\mathbf{S} = \{\mathbf{s}_1, \mathbf{s}_2, \dots, \mathbf{s}_n\}$  where  $\mathbf{s}_i$  and  $\mathbf{s}_{i+1}$  are segments next to each other. We compute the normal vectors of the segment at the middle point and scale them by half of the segment’s length. This is done to weigh the affordance effect this region carries. There are two affordance vectors per segment  $\mathbf{s}_i$ , each pointing in opposite directions, as depicted in Fig. 3(a). Let us define  $\mathbf{A} = \{\mathbf{a}_1, \mathbf{a}_2, \dots, \mathbf{a}_{2n}\}$  as the structure that contains all the affordance vectors  $\mathbf{a}_i$ , for  $n$  as the number of segments.

To determine which affordance vector  $\mathbf{a}_i$  will be used to interact with the manipulandum, we compare the similarity between  $\mathbf{a}_i$  and the vector from the manipulandum’s position

to the target point  $\mathbf{v}^{\text{target}}$  by:

$$\theta_i = \cos^{-1} \left( \frac{\mathbf{v}^{\text{target}} \cdot \mathbf{a}_i}{\|\mathbf{v}^{\text{target}}\| \|\mathbf{a}_i\|} \right) \quad (1)$$

where  $\theta_i$  is the similarity score. The optimal affordance vector  $\mathbf{a}_*$  and its according segment  $\mathbf{s}_*$  are found by:

$$\mathbf{a}_* = \arg \min_{\mathbf{a}} (\Theta) \quad \text{for } \Theta = \{\theta_1, \theta_2, \dots\} \quad (2)$$

where the vector with the minimum similarity score is the optimal affordance vector.

## 2.4 Manoeuvrability Analysis

A tool can push the manipulandum from the side, from the tip, or other areas. However, the relative location of the manipulandum respective to the tool affects its manoeuvrability. In other words, the affordance provided by the tool is proportional to manoeuvrability. Consider using a rotating stick to push an object with its end tip. In this situation, the tool may lose contact with the manipulandum as it rolls outwards, hence, the manoeuvrability of this point is low. On the other hand, the midpoint of the stick has a high manoeuvrability, which proportionally decreases as the contact point is further away from the midpoint. This behaviour can be modelled with a Gaussian function, where its centre is the segment's centre and the peak height is half the segment's length, see Fig. 3(b). We refer to this region as an affordance area.

All the pixels in the affordance area of  $\mathbf{s}_i$  are set to 1 in an image frame  $\mathbf{I}_i$  and the rest to 0, which creates a binary image; This process is repeated for all segments. All binary images are then summed as:

$$\hat{\mathbf{I}} = \sum_{i=1}^n \mathbf{I}_i, \quad [\mathbf{I}]_{x,y} = \begin{cases} 1, & \text{if it is an affordance area} \\ 0, & \text{else} \end{cases} \quad (3)$$

where  $n$  is the number of segments. The affordance of the tool segment is quantified with the (normalised) manoeuvrability matrix:  $\mathbf{M} = \hat{\mathbf{I}} / \hat{I}_{\max}$ , for  $\hat{I}_{\max}$  as the maximum value in  $\hat{\mathbf{I}}$ .

Tool regions with high values in the image  $\mathbf{M}$  reflect a high manoeuvrability. These computed manoeuvrability values are useful to determine the location where the tool interacts with the manipulandum. To determine the centre of the object, we then expand the contour of the tool by the object's radius  $r^{\text{obj}}$ . This contour is downsampled with the Ramer-Douglas-Peucker algorithm [44], then, parameterised with the spline fitting technique reported in [45]. To extract key features of the tool geometry, we use a sliding window strategy to examine a small number of neighbouring points. Let  $\mathcal{C}$  be the contour of the tool expanded by  $r^{\text{obj}}$ . The key features of the tool geometry are extracted using the following equation:

$$\mathcal{F} = \{p \in \mathcal{C} | \kappa(p) > \kappa_{\text{thresh}}\} \quad (4)$$

where  $\mathcal{F}$  is the set of feature points,  $p$  represents a point on the parameterized contour  $\mathcal{C}$ ,  $\kappa(p)$  is the curvature of the point  $p$ , and  $\kappa_{\text{thresh}}$  is a predefined curvature threshold. If there exists a point where its curvature is larger than a threshold in the local neighbourhood, we consider this point as one of the feature points.

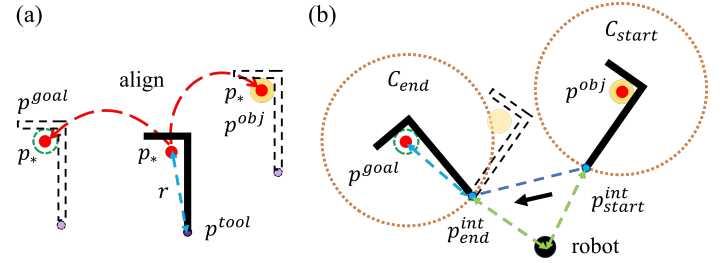


Figure 4: (a) The tool is virtually aligned to the current object and the goal location, with  $\mathbf{p}_* = \mathbf{p}^{\text{obj}}$  and  $\mathbf{p}_* = \mathbf{p}^{\text{goal}}$ . (b) The light blue dashed line is the radius of the orange circle  $\mathcal{C}_{\text{start}}$  and  $\mathcal{C}_{\text{end}}$ , which equals the distance between  $\mathbf{p}^{\text{tool}}$  and  $\mathbf{p}_*$ . The tool moves from  $\mathbf{p}_{\text{start}}^{\text{int}}$  to  $\mathbf{p}_{\text{end}}^{\text{int}}$  by following the dark blue dashed trajectory line.

To compute the minimal number of key points (denoted as  $\mathbf{P}^{\text{key}} = \{\mathbf{p}_1^{\text{key}}, \mathbf{p}_2^{\text{key}}, \dots\}$ ) that capture the highest manoeuvrability among feature points, we use the density-based clustering algorithm from [46]. By integrating the affordance areas we obtained earlier, we can filter out some redundant key points. For example, if there exists a point  $\mathbf{p}_i^{\text{key}}$  located outside the affordance area (visualised in Fig. 3(b)), we consider this point as redundant. All the non-redundant points are then grouped into  $\mathbf{P}^{\diamond} = \{\mathbf{p}_1^{\diamond}, \mathbf{p}_2^{\diamond}, \dots\}$ . To find the point in  $\mathbf{P}^{\diamond}$  with the highest manoeuvrability (defined as  $\mathbf{p}_*$ ), we use the manoeuvrability matrix  $\mathbf{M}$  and distance between  $\mathbf{p}_i^{\diamond}$  and  $\mathbf{a}_*$  as described in the metric below:

$$\mathbf{p}_* = \arg \min_{\mathbf{p}_i^{\diamond}} ((1 - [\mathbf{M}]_{\mathbf{p}_i^{\diamond}}) + \|\mathbf{p}_i^{\diamond} - \mathbf{a}_*\|) \quad (5)$$

where  $[\mathbf{M}]_{\mathbf{p}_i^{\diamond}}$  denotes to the image value of  $\mathbf{M}$  at point  $\mathbf{p}_i^{\diamond}$ . The region with the highest manoeuvrability is defined as the circle (with object radius) centred at  $\mathbf{p}_*$ . (see Fig. 3(b))

## 2.5 Manoeuvrability-Oriented Controller

The subtask “interact” triggers the robot to use the selected tool to drive the manipulandum towards the desired location. In this section, we derive our method to perform this type of motion assuming that the tool approaches the object and is going to make contact with it in the subtask “interact”.

**Initial and Final Poses.** The tool's pose corresponds to its grasping configuration, which coincides with the robot end-effector's pose when the robot grasps the tool (see Fig. 4).  $\mathbf{p}^{\text{tool}}$  denotes the tool's grasping point ( $x, y$  coordinates) when it has not come in contact with the object. To construct a trajectory for tool-based object transport, we need to find out the tool's desired initial and final poses for the subtask “interact”. We first define these poses (which include the orientation) of the chosen tool as  $\mathbf{p}_{\text{start}}^{\text{int}}$  and  $\mathbf{p}_{\text{end}}^{\text{int}}$  respectively.

To efficiently move the object, we propose a method that reduces the travel distance while ensuring continuous contact. In the first contact, we align the highest manoeuvrability point  $\mathbf{p}_*$  of the tool to the object's centre  $\mathbf{p}^{\text{obj}}$ , where  $\mathbf{p}_* = \mathbf{p}^{\text{obj}}$ .

The motion trajectory of a tool, moving along the z-axis of the object's centre without displacing it can be described as

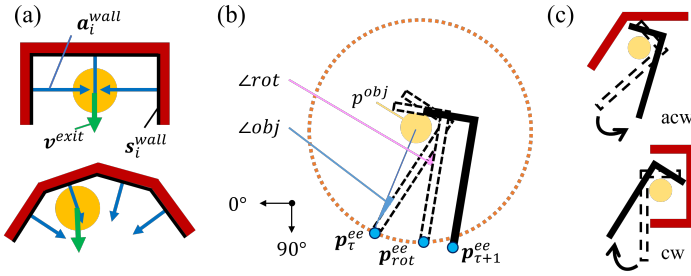


Figure 5: (a) Walls are in red with the segment of the wall  $\mathbf{s}_i^{\text{wall}}$  highlighted in black; blue arrows are the passive affordance vector and green arrows indicate the moving direction of  $\mathbf{v}^{\text{exit}}$ . (b) The tool pose moves from  $\tau$  to  $\tau + 1$  by rotating with  $\angle_{\text{rot}}$  and translating linearly to  $\mathbf{p}_{\tau+1}^{\text{ee}}$ . (c) Rotation direction of a tool: anti-clockwise and clockwise direction.

a circular trajectory with the centre  $\mathbf{p}^{\text{obj}}$  and radius  $r$ , where  $r = \|\mathbf{p}_* - \mathbf{p}^{\text{tool}}\|$ . The trajectories for the initial and final configurations are represented as  $\mathbf{C}_{\text{start}}$  and  $\mathbf{C}_{\text{end}}$  (see Fig. 4(a)).

The possible location for  $\mathbf{p}_{\text{start}}^{\text{int},x,y}$  will be lying on  $\mathbf{C}_{\text{start}}$  and can be determined by finding a point on  $\mathbf{C}_{\text{start}}$  which is the closest point to the robot (the distance is indicated with a light green dashed line in Fig.4(b)). Based on the tool’s geometry, we can determine the orientation of the initial pose  $\mathbf{p}_{\text{start}}^{\text{int}}$ ; The same approach applies to  $\mathbf{p}_{\text{end}}^{\text{int}}$ .

**Motion Strategy.** To stably move from  $\mathbf{p}_{\text{start}}^{\text{int}}$  to  $\mathbf{p}_{\text{end}}^{\text{int}}$ , the following motion strategy is implemented to achieve the task: First, the robot aligns  $\mathbf{p}_*$  with  $\mathbf{p}^{\text{obj}}$  and matches  $\mathbf{p}^{\text{tool}}$  with  $\mathbf{p}_{\text{start}}^{\text{int}}$  with the following equation:

$$\mathbf{p}^{\text{tool}} = \operatorname{argmin}_{\mathbf{p}} (f(\mathbf{p})) + \|\mathbf{p} - \mathbf{p}_{\text{start}}^{\text{int}}\| \quad (6)$$

where the coordinates of  $\mathbf{p}^{\text{tool}}$  can be determined by finding a point  $\mathbf{p} = (x, y)$  where it minimizes the distance between  $(\mathbf{p}_*, \mathbf{p}^{\text{obj}})$  with  $f(\mathbf{p})$  and  $(\mathbf{p}^{\text{tool}}, \mathbf{p}_{\text{start}}^{\text{int}})$ ; then translates along the  $x$  and  $y$  axes until it reaches  $\mathbf{p}_{\text{end}}^{\text{int},x,y}$  with  $k_{\text{int}}(\mathbf{p}_{\text{end}}^{\text{int},x,y} - \mathbf{p}^{\text{tool}})$ , where  $k_{\text{int}}$  is determined empirically; lastly, the tool is rotated to align with the orientation of  $\mathbf{p}_{\text{end}}^{\text{int}}$ .

## 2.6 Application with Environmental Constraints

When moving an object across a table, we may encounter constraints from the environment, such as walls. These constraints restrict the potential movement directions of the object. Formally, a constrained area can be defined by a series of points where more than one axis of freedom of the manipulum motion may be restricted. In this section, we focus on the motion triggered by the subtask ‘stepping’.

Consider the manipulum is tightly confined within a concave-shaped wall, as shown in Fig. 5(a), with an unknown exit and assume that the tool can enter the constrained area. To move the manipulum out from the bounded area with small movement space, we determine the direction from the manipulum to the exit by considering the overall affordance of the wall boundary. We denote this direction vector as  $\mathbf{v}^{\text{exit}}$ , and its magnitude is defined as the minimum travel

distance for the manipulum. Consider the inner edge of the wall as a segment  $\mathbf{s}_i^{\text{wall}}$  where  $i = \{1, \dots, n^{\text{wall}}\}$  and  $n^{\text{wall}}$  is the number of the wall segment. The affordance of a wall is passively provided and is defined as  $\mathbf{a}_i^{\text{wall}}$  with the model shown in Sec. 2.3. The passive affordance vector is the normal vector of  $\mathbf{s}_i^{\text{wall}}$  located in the middle with the direction pointing towards the constrained area. Its magnitude is scaled to half of  $\mathbf{s}_i^{\text{wall}}$  as the manipulum is generally not receiving any affordance from a wall segment based on our visual affordance model. The moving direction for the manipulum to the exit can be obtained by the following equation:

$$\mathbf{v}^{\text{exit}} = \sum_{i=1}^{n^{\text{wall}}} \mathbf{a}_i^{\text{wall}} + \mathbf{p}^{\text{obj}} \quad (7)$$

where  $\mathbf{v}^{\text{exit}}$  integrates all passive wall affordance vectors  $\mathbf{a}_i^{\text{wall}}$  with the current position of the manipulum, see 5(a).

Given that only part of the tool can enter the confined area, our primary focus is the tip of the tool. The segment connecting of the tool’s tip is denoted as  $\mathbf{s}^{\text{tip}}$ , with its corresponding affordance vector denoted as  $\mathbf{a}^{\text{tip}}$ . The desired rotation angle of the end pose of  $\mathbf{a}^{\text{tip}}$  is the angle of  $\mathbf{v}^{\text{exit}}$ .

The highest manoeuvrability region can be obtained by treating  $\mathbf{v}^{\text{exit}}$  as the target vector  $\mathbf{v}^{\text{target}}$ ,  $\mathbf{a}^{\text{tip}}$  as the desired affordance  $\mathbf{a}_*$ , and assuming the tool is rotated such that  $\mathbf{a}^{\text{tip}} = b\mathbf{v}^{\text{exit}}$  with  $b > 0$  as a scaling factor. We first align  $\mathbf{s}^{\text{tip}}$  to the first segment of the wall (i.e.  $\mathbf{s}_1$ ), with  $\mathbf{p}^{\text{obj}}$  inside the highest manoeuvrability region of the tool. The tool approaches the object and maintains contact with the manipulum by minimising the distance  $\|\mathbf{p}_* - \mathbf{p}^{\text{obj}}\|$ .

To move in the limited area while interacting with the manipulum, we employ a stepping approach to manipulate the manipulum in the confined area. As the possible movement area is small and highly restricted, an incremental pulsing motion is adopted to make small adjustments with high accuracy motion control to the tool and the manipulum. Inspired by the animal manipulation study in [4] (where a crow uses a tool to get the food from the box slot by rotating and dragging the tool outwards), we adopt a similar approach to retrieve the object from confined spaces. This strategy continuously alternates between ‘repositioning’ the tool and incremental ‘rotation-dragging’ the object towards the exit until it can be fully extracted as depicted in Fig. 5.

We define ‘repositioning’ as moving the tool closer to the object and realigning  $\mathbf{p}_*$  with  $\mathbf{p}^{\text{obj}}$  by  $k$  amount. The value of  $k$  is determined empirically. In ‘rotation-dragging’, the tool maintains contact with the manipulum when it rotates by a certain angle as  $\angle_{\text{rot}}$  shown in Fig. 5(b) and moves outwards by extending  $\overrightarrow{\mathbf{p}_{\tau}^{\text{ee}} \mathbf{p}_{\text{rot}}^{\text{ee}}}$  by a  $w > 0$  amount.

$\tau$  is an action step variable and is incremented by 1 if an action (reposition/rotation-dragging) is fulfilled (i.e.  $\tau = 0, 1, 2, \dots$ ). To control the change of action, a step function (denoted as  $u(\tau)$ ) is implemented as a trigger with the step variable  $\tau$ . This kind of non-prehensile crow-inspired

behaviour can be unified and modelled as:

$$\mathbf{p}_{\tau+1}^{\text{ee}} = \begin{bmatrix} \mathbf{p}_{\tau}^{\text{ee},x} \\ \mathbf{p}_{\tau}^{\text{ee},y} \\ \phi_{\tau} \end{bmatrix} + u(\tau) \begin{bmatrix} k(\mathbf{p}_{\tau}^{\text{obj},x} - \mathbf{p}_{*}^x) \\ k(\mathbf{p}_{\tau}^{\text{obj},y} - \mathbf{p}_{*}^y) \\ 0 \end{bmatrix} + u(\tau+1) \begin{bmatrix} w(\mathbf{p}_{\tau}^{\text{obj},x} - r \cos(\phi_{\tau}) - \mathbf{p}_{\tau}^{\text{ee},x}) \\ w(\mathbf{p}_{\tau}^{\text{obj},y} + r \sin(\phi_{\tau}) - \mathbf{p}_{\tau}^{\text{ee},y}) \\ f(\phi_{\tau+1}) \end{bmatrix}$$

$$u(\tau) = \begin{cases} 0, & \text{if } \tau \text{ is odd} \\ 1, & \text{if } \tau \text{ is even} \end{cases} \quad (8)$$

where  $\mathbf{p}_{\tau+1}^{\text{ee}}$  is the next target pose of the end-effector at the action step  $\tau+1$  for the affordance vector  $\mathbf{a}^{\text{tip}}$  not parallel to  $\mathbf{v}^{\text{exit}}$ , such that  $\mathbf{a}^{\text{tip}} \neq b\mathbf{v}^{\text{exit}}$ . The angle of the tool at  $\tau+1$  (denoted as  $\phi_{\tau+1}$ ) depends on the rotational direction (see Fig. 5), that  $\phi_{\tau+1}$  is computed as

$$f(\phi_{\tau+1}) = \begin{cases} -\angle\text{obj} - \angle\text{rot}, & \text{if direction is anti-clockwise} \\ -\phi_{\tau} + \pi - \angle\text{obj} - \angle\text{rot}, & \text{otherwise} \end{cases} \quad (9)$$

where  $\phi_{\tau}$  is the tool's angle at the action step  $\tau$ ,  $\angle\text{obj}$  is the angle between the manipulandum, grasping point, and a tool's keypoint,  $\angle\text{rot}$  is the amount of angle to rotate.

### 3 Results

To validate our methodology in terms of accuracy and robustness, we have conducted around 200 experiments in a dual-arm robot system. In the experiment, two sets of UR-3 robotic arms are used and GPT 4o-mini is implemented for task decomposition. Three types of tools are selected which are a stick, an L-shaped hook, and a Y-shaped hook (see Fig.1). Different tool combinations are evaluated with diverse movement directions and tasks. Various masses of the manipulandum are tested and validated. Since this is a vision-based controller, the mass of the manipulandum does not significantly affect the results. Therefore, the manipulandum's mass is omitted from this section. A RealSense D415 captures the images of the whole process. Data is passed to a Linux-based computer with the Robot Operating System (ROS) for image process and robot control. Aruco code is used for providing accurate pose tracing in real time. The average inference time is approximately 0.158 seconds for tool analysis and around 1.51 seconds for LLM processing. Since these operations are completed before the robot begins its movements, their effect on overall system responsiveness remains minimal.

These experiments include validating the task decomposition performance in a single and dual-arm robot setup, the robustness of the affordance and manoeuvrability model in various shapes of tools, and evaluating the overall performance.

#### 3.1 Single-Arm Robot with a Single Tool

We first evaluate the task decomposition performance of LLM. For that, a tool and a blue manipulandum are placed on the table with the target given as shown in Fig. 6. The task is to manipulate the manipulandum within a close distance, which is sufficient for a single-arm robot. The embedded information which contains the task, the environment, and the geometry of the tool is passed to the LLM.

In the experiment shown in Fig. 6(a), the robot executes the subtasks generated by the high-level symbolic task planner which include: `grasp(right, hook)`; `approach(right, hook, block)`; `interact(right, hook, block, target)`; `release(right, hook)`. where the right arm first moves and grasps the hook, then moves the block to the target, and lastly releases the tool back to its original place. In a non-single tool scenario, where two tools are available on the desk as shown in Fig. 6(c), the task planner selects the nearest tool based on the embedded information to push the block towards the target. The experiment showcases the application of the proposed affordance and manoeuvrability model in locating the highest manoeuvrability region for manipulandum transportation. During the manipulation stage, the manipulandum is kept within the highest manoeuvrability region (indicated with a red circle in Fig. 6) to receive affordance effectively from the tool. The minimisation of the error between the  $\mathbf{p}^{\text{obj}}$  and the  $\mathbf{p}^{\text{target}}$  for each experiment is shown in Fig. 7. These results corroborate that the proposed method can be used to actively drive a robot to manipulate an object via a tool.

#### 3.2 Dual-Arm Robot with Long-Horizon Task

We then evaluate the long-horizon task performance where the manipulandum has to travel from far right to far left, far right/left to top right/left, and vice versa. The long-horizon task is evaluated with multiple tool combinations. The system observes and generates a collaborative motion plan. In the experiment shown in Fig. 8(a), the right and left arms pick up the stick and the hook respectively. The right arm uses the stick to push the manipulandum to the left side, allowing the left arm to continue the task. The robot leverages the advantage of the hook to drag the manipulandum closer to its working area and push the manipulandum to the desired location. In Fig. 8(b), the right and left arms grasped the Y-shaped tool and the stick respectively. The right arm uses the tool to pass the manipulandum to the left. The left arm uses the stick to push the manipulandum to the target location.

The long-horizon task performance is evaluated with the tool-sharing ability. Assuming there is only one tool available, it has to be shared among the dual-arm robot. Fig. 8(c) demonstrates the tool is passed to another arm once the manipulandum is pushed to the middle of the table. The manipulandum is moved accurately to the target with motion-decomposed: `'grasp; approach; interact; pass; release; grasp; approach; interact; release'` where the left arm releases the tool once it is done and the right picks up the tool to continue moving the manipulandum. Though the hook is in a two-link geometry, the pushing is afforded by the right side of the tool (a single segment) with the highest manoeuvrability region.

The minimisation of the error between  $\mathbf{p}^{\text{obj}}$  and  $\mathbf{p}^{\text{target}}$  for each experiment is shown in Fig. 9. Similar to the single-arm robot with a single tool experiment, this long-horizon task also demonstrates the robustness of the proposed methodology such that the tasks are successfully decomposed into multiple collaborative subtasks, and the highest manoeuvrability region of the tool is leveraged in manipulandum manipulation.

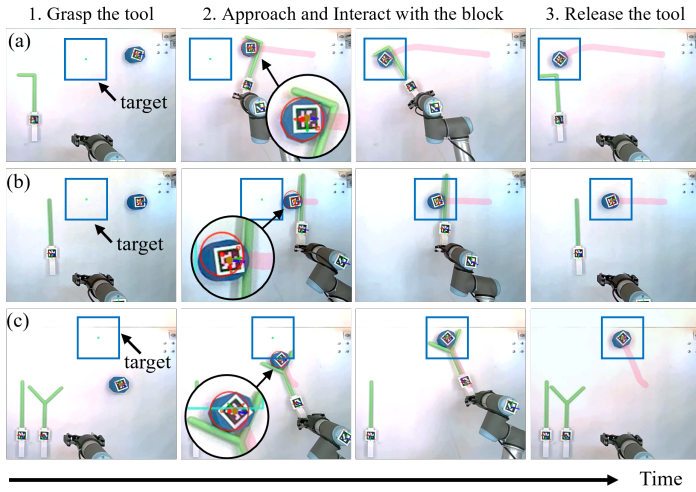


Figure 6: Single-arm robot with a single tool: moving the manipulandum (a) right to left with a hook, (b) right to left with a stick, and (c) bottom to top with a Y-shaped tool. The red line shows the manipulandum’s trajectory, while the red circle indicates the highest maneuverability point.

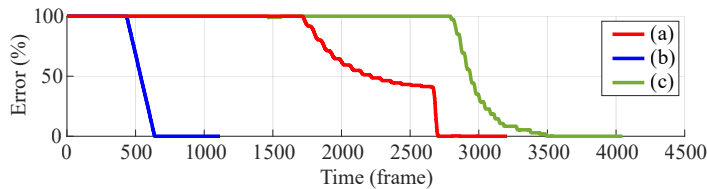


Figure 7: Evolution of the minimisation process of the error between the current object position and the target for the tasks shown in Fig. 6.

### 3.3 Tool-Object Manipulation in Constrained Environments

To further evaluate the performance of the model in application scenarios, different shapes of walls are constructed as shown in Fig. 8(d)–(e). Two walls are designed with 90-degree and 65-degree for the inner-angles. Maneuvering a hook within a confined space presents greater challenges compared to using a stick. Additionally, a Y-shaped hook proves unsuitable for dragging objects in tight quarters. Therefore, in this experimental study, we opt for a hook tool with a right arm to navigate effectively within the constrained environment. Similar to the previous results, Fig. 8(d)–(e) also implements the task planner successfully to decompose the task and applies the stepping controller for object manipulation. The tool first aligns its  $\mathbf{s}^{\text{tip}}$  to the first segment of the wall and adopts the proposed non-prehensile stepping motion controller stated in (8). The manipulandum is dragged out from the confined area by alternating between the action of ‘repositioning’ and ‘rotation-dragging’.

During the pulsing manipulation, the manipulandum maintains contact with the highest manoeuvrability region. The contact changes between the centre of the highest manoeuvrability region  $\mathbf{p}_*$  with the manipulandum is visualized in Fig. 10(a). The error between the  $\mathbf{p}^{\text{obj}}$  and the wall exit for each experiment are minimised with time, as shown in Fig. 9.

### 3.4 Comparison

We analyze the affordance utilization and provision for the selected tools by assessing the frequency of contact between the manipulandum and the tool segments. In the majority of instances, the manipulandum interacts with the affordance primarily in the red region, as indicated in Fig. 10(b) and aligns closely with our proposed model.

We compare our system with other state-of-the-art methods. In terms of LLM-based task decomposition, we assess the success rates of our approach with zero-shot and few-shot learning methods [48], DELTA [25], SayPlan [47], and fine-tuning on a smaller dataset, as shown in Fig. 11(a). In the comparison, zero-shot and few-shot learning refer to using prompts solely with a pre-trained model, rather than with a fine-tuned model. We consider task decomposition successful only if the output is optimal, with no unnecessary or redundant steps.

We observe that, under the same conditions, prompting (zero-shot and few-shot learning) is relatively unreliable, particularly in long-horizon tasks. This unreliability may stem from the insufficient number of manipulation examples provided in the prompt. Similarly, even when more information is given through domain knowledge and graphs [25, 47], the LLM still struggles to generate a reasonable list for tasks involving both arms.

Fine-tuning a model with a smaller dataset (200 examples) yields acceptable results; however, it occasionally introduces unnecessary or infeasible steps in long-horizon tasks. In general, most methods demonstrate relatively positive outcomes in single-arm, single-tool tasks (SRST and TOME), likely due to the simplicity of these tasks. Specifically, the focus is on extracting the manipulandum from a constrained environment rather than aiming for a specific destination, and coordination between arms can be omitted. In summary, utilizing a larger dataset for fine-tuning results in enhanced task decomposition performance, leading to more consistent outcomes.

We assess the tool analysis method by identifying the highest manoeuvrability point across 32 tool images, with the results outlined in Fig. 11(b) and 12. The center of the manipulated manipulandum is taken as the ground truth. For our analysis, we consider the average error, root mean square error (RMSE), and mean absolute error (MAE) as the key metrics. The results are visualized in Fig. 12, showcasing the differences between the ground truth and the computed results under various methodologies. In the comparison, we observe that the total variation regularization (TVR) method [49] had a relatively higher difference from the ground truth. The keypoint-inspired learning approach (similar to [50]) yields comparable results to our method. However, the keypoint approach requires manual labelling of large amounts of data and model training, and its accuracy is highly dependent on the quality of the dataset. As shown in Fig. 12, both the keypoint and our methods had lower errors along the x-axis than the y-axis. Overall, both achieved relatively lower errors than the TVR method. Yet, in general, our proposed method demonstrated more stable performance and higher accuracy in terms of manoeuvrability computation.

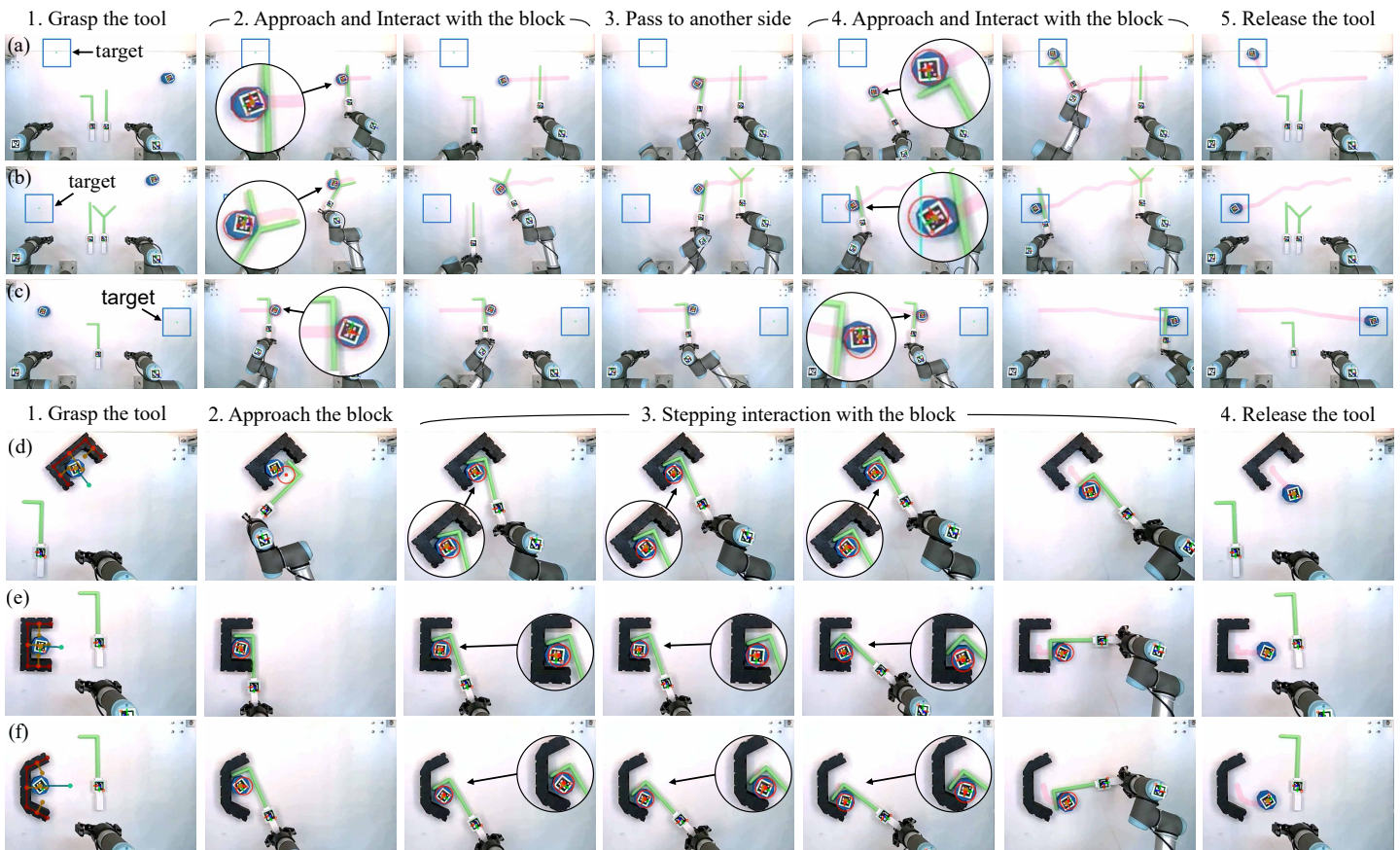


Figure 8: Long-horizon task: moving the manipulum from (a) far right to far left with a hook and a stick, (b) far top right to far left with a stick and a Y-shaped tool, (c) far left to far right with a hook; and (d)–(f) exit from a confined area with a stepping controller. The manipulum trajectory is reflected in pink and the target is labelled with a blue square.

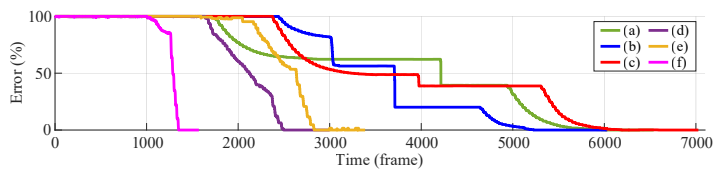


Figure 9: Evolution of the minimisation process of the error between the current object position and the target for the tasks shown in Fig. 8.

## 4 Conclusion

In this paper, we present a new manoeuvrability-driven approach for tool-object manipulation. The LLM is integrated for task decomposition, generating collaborative motion sequences for a dual-arm robot system. A compact geometrical-based affordance model for describing the potential functionality and computing the highest manoeuvrability region of a tool is developed. A non-prehensile motion controller and a stepping manipulation model are derived for TOM and incremental movements in a constrained area. Experimental results are reported and analysed for the proposed methodology validation. We illustrate the performance of the proposed methods in the accompanying video <https://vimeo.com/917120431> and in the webpage [https://samanthalhy.github.io/tool\\_manipulation/](https://samanthalhy.github.io/tool_manipulation/).

Our method introduces a new affordance and manoeuvra-

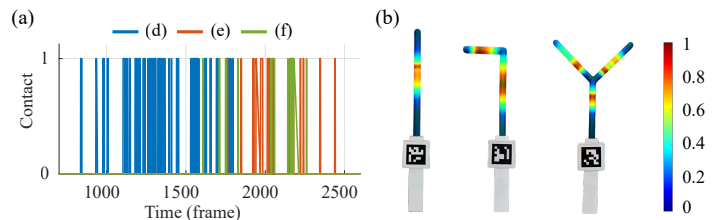


Figure 10: (a) Stepping movement evolution of the change in contact between the manipulum and the highest manoeuvrability point for the tasks shown in Fig. 8(d)–(f). 1 refers to in-contact and 0 refers to no contact. (b) Contact frequency of a segment side: regions depicted in deeper red indicate higher contact frequency with the manipulum and a higher occurrence of affordance provision.

bility paradigm for tool-based object manipulation. To obtain a better performance, we split the model into task decomposition and mathematical motion models. However, the logical fault in the LLM’s response may be unseen and thus lead to inappropriate motion. In our experiments, there are a few times that the LLM presents infeasible plans. Moreover, the current affordance model presents promising results with simple geometrical shapes. Dynamics shapes like deformable objects may be complicated to perform accurate modelling. In terms of manoeuvrability, it may be complicated to compute an accurate result for scenes with unstable illumination, low

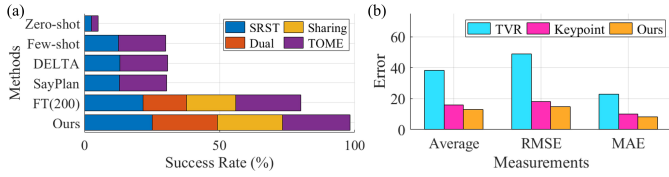


Figure 11: Comparison of (a) success rate and (b) accuracy of tool manoeuvrability points under different state-of-the-art methodologies. FT states for fine-tuning, SRST states for a single-arm robot with a single tool, Dual refers to dual arms collaboration with two tools, and Sharing refers to tool-sharing collaboration. DELTA is the few-shot learning with domain adaptation [25] and SayPlan is from [47].

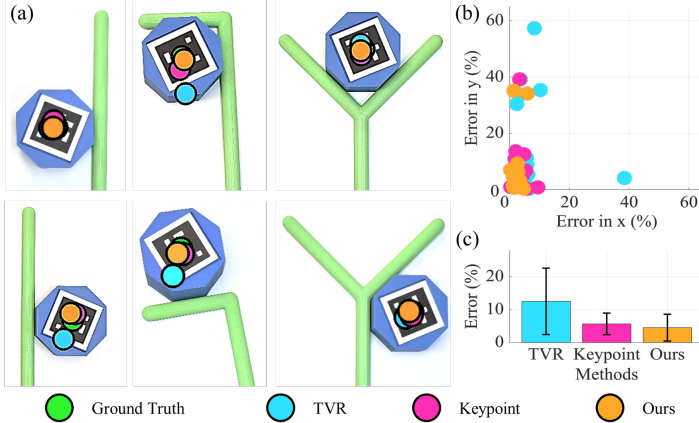


Figure 12: Comparison of tool maneuverability points under different state-of-the-art methodologies: Green circles represent the ground truth, while blue, pink, and orange denote the computed results of the total variation regularization method, keypoint-inspired learning method, and our method respectively. (a) Differences visualization; (b) the average error between ground truth and computed results along the x and y axes in percentage; (c) general differences in percentage.

contrast in images, large height differences in objects (tools and the manipulandum), etc. We simplified these cases using ArUco code for real-time object tracking in the experiments.

For future work, we would like to extend our method to deal with multiple object transportation and manipulation with tools. We would also like to perform deformable object manipulation, e.g., in the case of manipulating objects with ropes or fabrics. Also, we would like to test the performance of our controller but using other models. For that, the stability of the controller might be needed. We encourage readers to work on this open problem.

## 5 Appendix

### 5.1 LLM-Based High-Level Symbolic Task Planner

The training data for fine-tuning an LLM is generated with the pose of the robots, tools, block, and target randomly assigned based on the task description. The available motion functions are listed in Table 1.

Under various scenarios, the input and output of the task planner are illustrated in Fig. 13, 14, 15, where  $x$  and  $y$  refer to the coordinates of the items, such as the position of the block. The instructions and scene information are embedded to form the input for the planner. The scene information includes the positions of the robots, tools, block, target, and the key points of the tools and walls (if applicable).

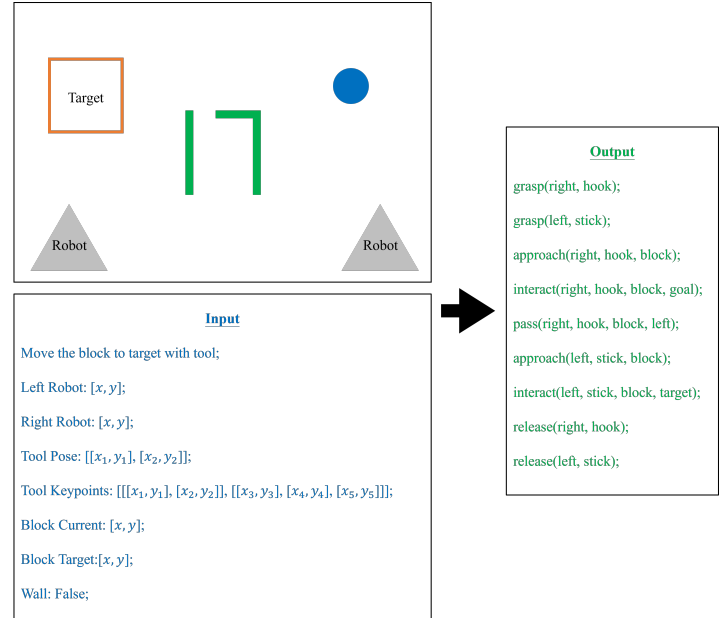


Figure 13: The input and output of the task planner for a long-horizon task with two tools. The input prompt is composed of the task instruction, the coordinates of robots, tools, and the block. The generated task sequence: first grasps both tools, then manipulates the block from right to the target location, and returns both tools to their original location.

## 5.2 Additional Experiments

### Different Tools in a Long Horizon Task

- Case 1: Using a stick and then a hook to push the blue block to a faraway target, from right to left (see Fig. 16).
- Case 2: Using a stick and then a hook to push the blue block to a faraway top location, from left to top-right (see Fig. 17).
- Case 3: Using a Y-shaped hook and then a stick to push the blue block to the left-hand side target, from top-right to left (see Fig. 18).

### Single Tool in a Long Horizon Task: Tool Sharing

- Case 4: Using a hook to push the blue block to a faraway target, from right to left (see Fig. 19).
- Case 5: Using a hook to push the blue block to the top-right location, from center-left to top-right (see Fig. 20).

### Manipulation in a Constrained Environment

Table 1: Motion Functions Available

Function	Description
<code>grasp(<i>arm</i>, <i>tool</i>)</code>	To grasp a <i>tool</i> with the robot <i>arm</i> .
<code>approach(<i>arm</i>, <i>tool</i>, <i>m</i>)</code>	To approach the location of <i>m</i> with <i>tool</i> using <i>arm</i> .
<code>interact(<i>arm</i>, <i>tool</i>, <i>m</i>, <i>goal</i>)</code>	To move <i>m</i> to the <i>goal</i> location with the <i>tool</i> .
<code>stepping(<i>arm</i>, <i>tool</i>, <i>m</i>)</code>	To move <i>m</i> out from the bounded area with the <i>tool</i> of the <i>arm</i> through contact pulsing motions.
<code>pass(<i>arm1</i>, <i>tool</i>, <i>m</i>, <i>arm2</i>)</code>	To pass <i>m</i> to another arm’s workspace.
<code>release(<i>arm</i>, <i>tool</i>)</code>	To release the <i>tool</i> back to its original place with the <i>arm</i> .

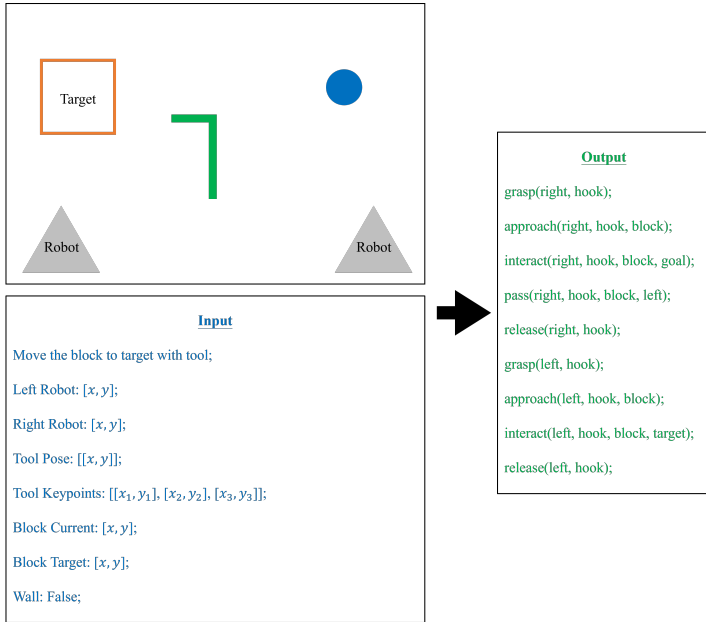


Figure 14: The input and output of the task planner for a long-horizon task with a single tool. The input prompt is composed of the task instruction, the coordinates of robots, tools, and the block. The generated task sequence: first grasps the tool with the right arm, then passes the block from the right to the left side, and puts the tool back to its original location once the block is at the target location.

- Case 6: Using a hook to get the blue block out from a constrained environment (see Fig. 21).
- Case 7: Using a hook to get the blue block out from a constrained environment with a different configuration (see Fig. 22).

### 5.3 Comparative Analysis of Task Decomposition Methodologies

In this section, we present a comparative analysis of various methodologies employed for robot task planning, specifically focusing on their success rates in different task scenarios. The methodologies evaluated include Zero-shot learning, Few-shot learning, DELTA [25], SayPlan [47], planning domain definition language (PDDL) [18], behaviour tree [19], and Fine-tuning with 200 data, and our proposed approach. The results are summarized in Table 2. Scenarios Evaluated:

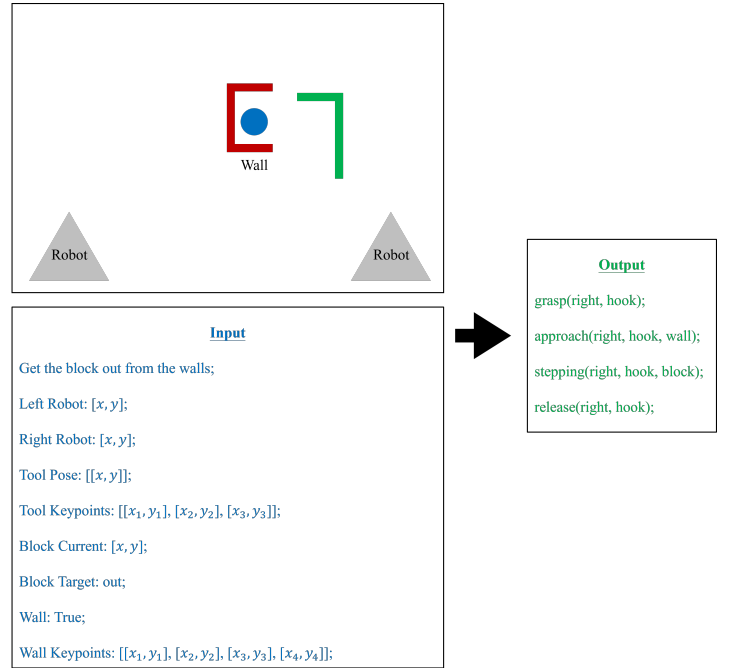


Figure 15: The input and output of the task planner with environmental constraints. The input prompt is composed of the task instruction, the coordinates of robots, tools, the block, and the wall. The generated task sequence: first grasps the hook, then incrementally controls the tool to drag the block out from the constrained area, and returns the hook to its original location.

- Our experiment setting: The position of the robot, tools, block, and target are based on our experiment settings
- New Case 1: New language instruction with the positions are based on a slightly larger table and robot’s workspace settings.
- New Case 2: New language instruction with the positions are based on a random-sized table and the robot’s workspace settings.

In our experiment setting, most methods performed well, with PDDL and Behavior Trees achieving the highest initial success rates. However, they struggled in more complex scenarios, indicating limited generalizability. In New Case 1, our proposed method maintained a high success rate of 0.97, while PDDL and Behavior Tree approaches dropped to 0.42, highlighting their challenges in adapting to new instructions. Specifically, when the setting was expanded to twice the orig-

Table 2: Success Rate Comparison in Task Decomposition

Methods	Our experiment setting	New Case 1	New Case 2	Overall(%)
Zero-shot learning	0.05	-	-	1.67%
Few-shot learning	0.30	0.24	0.13	22.3%
DELTA [25]	0.31	0.26	0.14	23.7%
SayPlan [47]	0.31	0.25	0.14	23.0%
PDDL [18]	0.99	0.42	0.06	49.0%
Behaviour tree [19]	0.99	0.42	0.04	48.3%
Fine-tuning (200 data)	0.83	0.77	0.69	76.3%
Ours	0.98	0.97	0.95	96.7%

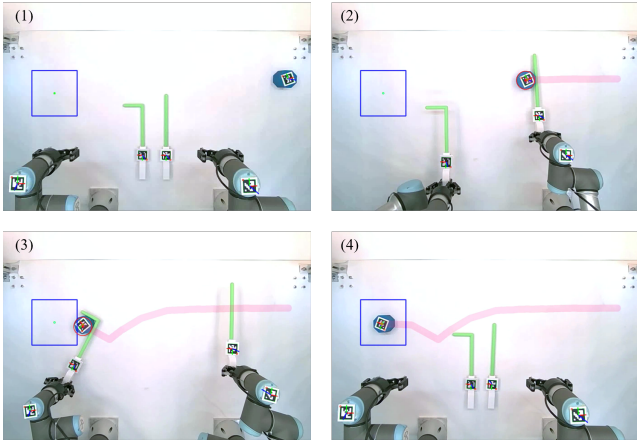


Figure 16: Case 1: (1) Observe the scene; (2) grasp and use the stick to push the blue block to the centre to pass it to the left arm; (3) use the hook to push the blue block to the target; (4) the blue block is at the desired location and both tools are put back to their original place.

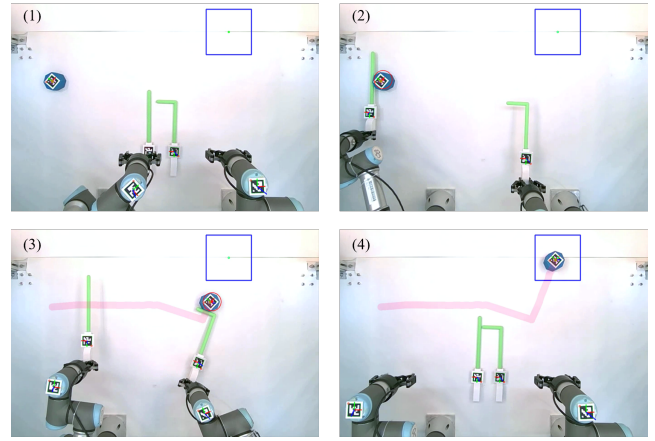


Figure 17: Case 2: (1) Observe the scene; (2) grasp and use the stick to push the blue block to the centre to pass it to the left arm; (3) use the top part of the hook to push the blue block to the top-right location; (4) the blue block is at the desired location and both tools are put back to their original place.

inal size, the rules and conditions in PDDL and Behavior Trees proved ineffective. For instance, one condition stipulated that if the distance between the block and the right arm was less than a specified amount, then the right arm would move. However, as the workspace was enlarged, these conditions remained based on the original setting, resulting in no response from the system in some situations since none of the conditions were fulfilled.

A similar trend was observed in New Case 2, where our approach achieved an impressive success rate of 0.95, while other methods demonstrated lower effectiveness and adaptability. In general, fine-tuning can effectively adapt to new settings primarily because it can interpret new instructions from the prompt input and adjust its output accordingly. Overall, the fine-tuning method achieves superior results due to its high adaptability and generalizability to new instructions.

## References

- [1] A. Stoytchev, *Robot tool behavior: A developmental approach to autonomous tool use*. Georgia Institute of Technology, 2007.
- [2] A. Z. Ren, B. Govil, T.-Y. Yang, K. R. Narasimhan, and A. Majumdar, “Leveraging language for accelerated learning of tool manipulation,” in *Conf. on Robot Learning*, pp. 1531–1541, 2023.
- [3] E. S. Reed, “Applying the theory of action systems to the study of motor skills,” in *Advances in psychology*, vol. 50, pp. 45–86, Elsevier, 1988.
- [4] D. E. McCoy, M. Schiestl, P. Neilands, R. Hassall, R. D. Gray, and A. H. Taylor, “New caledonian crows behave optimistically after using tools,” *Current Biology*, vol. 29, no. 16, pp. 2737–2742, 2019.
- [5] L. Jamone, “Modelling human tool use in robots,” *Nature Machine Intelligence*, vol. 4, no. 11, pp. 907–908, 2022.
- [6] H. Huang, C. Zeng, L. Cheng, and C. Yang, “Toward generalizable robotic dual-arm flipping manipulation,” *IEEE TIE*, 2023.
- [7] S. Y. Shin and C. Kim, “Human-like motion generation and control for humanoid’s dual arm object manipulation,” *IEEE TIE*, vol. 62, no. 4, pp. 2265–2276, 2014.
- [8] X. Wu and Z. Li, “Cooperative manipulation of wearable dual-arm exoskeletons using force communication between partners,” *IEEE TIE*, vol. 67, no. 8, pp. 6629–6638, 2019.

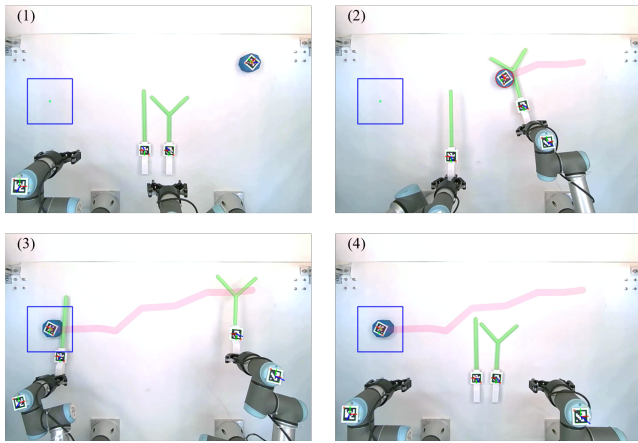


Figure 18: Case 3: (1) Observe the scene; (2) the right arm grasps and uses the left side of the Y-shaped hook to push the blue block closer to the left arm; (3) the left arm uses the left side of the stick to continue pushing the blue block to the target location; (4) the blue block is at the desired location and the tools are returned to its original place.

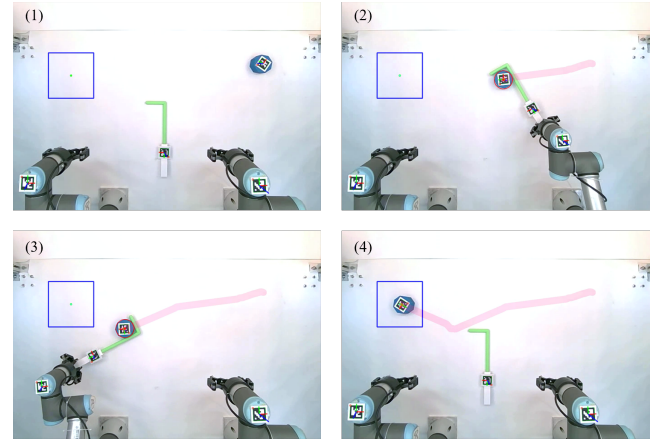


Figure 19: Case 4: (1) Observe the scene; (2) the right arm grasps and uses the hook to push the blue block to the centre to pass it to the left arm; (3) the right arm releases the hook and the left arm uses the inner part of the hook to manipulate the blue block to the target location; (4) the blue block is at the desired location and the hook is returned to its original place.

- [9] M. Qin, J. Brawer, and B. Scassellati, “Robot tool use: A survey,” *Frontiers in Robotics and AI*, vol. 9, p. 1009488, 2023.
- [10] O. Kroemer, S. Niekum, and G. Konidaris, “A review of robot learning for manipulation: Challenges, representations, and algorithms,” *The Journal of Machine Learning Research*, vol. 22, no. 1, pp. 1395–1476, 2021.
- [11] M. T. Mason, “Toward robotic manipulation,” *Annual Review of Control, Robotics, and Autonomous Syst.*, vol. 1, pp. 1–28, 2018.
- [12] H.-Y. Lee, P. Zhou, B. Zhang, L. Qiu, B. Fan, A. Duan, J. Tang, T. L. Lam, and D. Navarro-Alarcon, “A distributed dynamic framework to allocate collaborative tasks based on capability matching in heterogeneous multi-robot systems,” *IEEE Trans. on Cognitive and Developmental Syst.*, 2023.
- [13] Y. Jiang, F. Yang, S. Zhang, and P. Stone, “Task-motion planning with reinforcement learning for adaptable mobile service robots,” in *2019 IEEE/RSJ International Conference on Intelligent Robots and Systems (IROS)*, pp. 7529–7534, IEEE, 2019.
- [14] L. Marzari, A. Pore, D. Dall’Alba, G. Aragon-Camarasa, A. Farinelli, and P. Fiorini, “Towards hierarchical task decomposition using deep reinforcement learning for pick and place subtasks,” in *2021 20th International Conference on Advanced Robotics (ICAR)*, pp. 640–645, IEEE, 2021.
- [15] G. Kwon, B. Kim, and N. K. Kwon, “Reinforcement learning with task decomposition and task-specific reward system for automation of high-level tasks,” *Biomimetics*, vol. 9, no. 4, p. 196, 2024.
- [16] C. Son, “Intelligent rule-based sequence planning algorithm with fuzzy optimization for robot manipulation tasks in partially dynamic environments,” *Information Sciences*, vol. 342, pp. 209–221, 2016.
- [17] S. Veer, A. Sharma, and M. Pavone, “Multi-predictor fusion: Combining learning-based and rule-based trajectory predictors,” in *Conference on Robot Learning*, pp. 2807–2820, PMLR, 2023.
- [18] J. Jeon, H.-r. Jung, F. Yumbla, T. A. Luong, and H. Moon, “Primitive action based combined task and motion planning for the service robot,” *Frontiers in Robotics and AI*, vol. 9, p. 713470, 2022.
- [19] J. A. Bagnell, F. Cavalcanti, L. Cui, T. Galluzzo, M. Hebert, M. Kazemi, M. Klingensmith, J. Libby, T. Y. Liu, N. Pollard, *et al.*, “An integrated system for autonomous robotics manipulation,” in *2012 IEEE/RSJ International Conference on Intelligent Robots and Systems*, pp. 2955–2962, IEEE, 2012.
- [20] N. Wake, A. Kanehira, K. Sasabuchi, J. Takamatsu, and K. Ikeuchi, “Gpt-4v (ision) for robotics: Multimodal task planning from human demonstration,” *arXiv preprint arXiv:2311.12015*, 2023.
- [21] M. Ahn, A. Brohan, N. Brown, Y. Chebotar, O. Cortes, B. David, C. Finn, C. Fu, K. Gopalakrishnan, K. Hausman, *et al.*, “Do as i can, not as i say: Grounding language in robotic affordances,” *arXiv preprint arXiv:2204.01691*, 2022.
- [22] W. Huang, F. Xia, T. Xiao, H. Chan, J. Liang, P. Florence, A. Zeng, J. Tompson, I. Mordatch, Y. Chebotar, *et al.*, “Inner monologue: Embodied reasoning through planning with language models,” *arXiv preprint arXiv:2207.05608*, 2022.
- [23] I. Singh, V. Blukis, A. Mousavian, A. Goyal, D. Xu, J. Tremblay, D. Fox, J. Thomason, and A. Garg, “Prog-prompt: Generating situated robot task plans using large

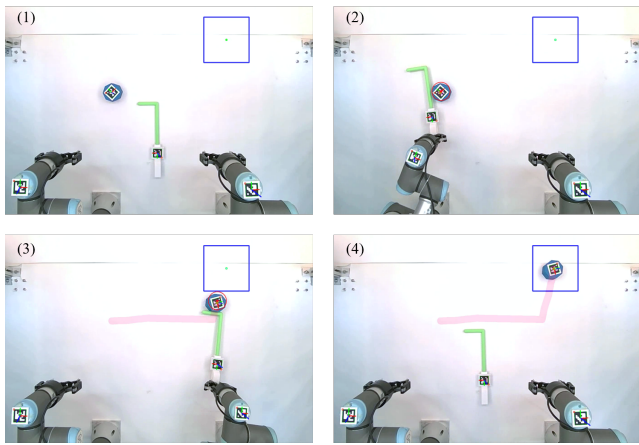


Figure 20: Case 5: (1) Observe the scene; (2) the left arm grasps and uses the right side of the hook to push the blue block closer to the right arm; (3) the left arm releases the hook and the right arm uses the top part of the hook to push the blue block to the target location; (4) the blue block is at the desired location and the hook is returned to its original place.

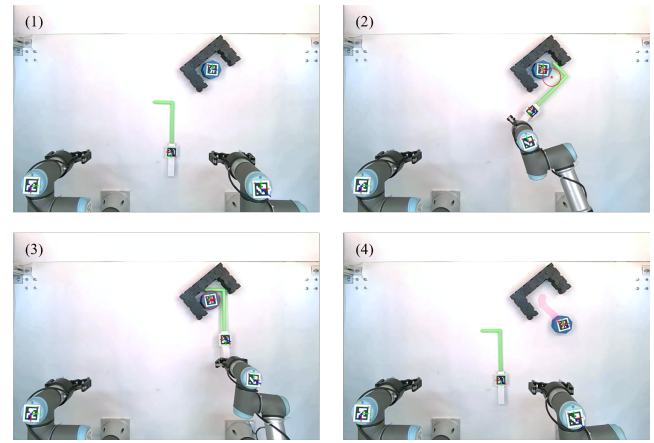


Figure 21: Case 6: (1) Observe the scene; (2) the right arm grasps the hook and approaches the blue block by aligning the top part of the tool to the wall; (3) the blue block is dragging out slowly with the hook being repositioned and rotation-dragging; (4) the blue block is moved out and the hook is returned to its original place.

language models,” in *IEEE ICRA*, pp. 11523–11530, 2023.

- [24] J. Liang, W. Huang, F. Xia, P. Xu, K. Hausman, B. Ichter, P. Florence, and A. Zeng, “Code as policies: Language model programs for embodied control,” in *IEEE ICRA*, pp. 9493–9500, 2023.
- [25] Y. Liu, L. Palmieri, S. Koch, I. Georgievski, and M. Aiello, “Delta: Decomposed efficient long-term robot task planning using large language models,” *arXiv preprint arXiv:2404.03275*, 2024.
- [26] J. Wu, R. Antonova, A. Kan, M. Lepert, A. Zeng, S. Song, J. Bohg, S. Rusinkiewicz, and T. Funkhouser, “Tidybot: Personalized robot assistance with large language models,” *arXiv preprint arXiv:2305.05658*, 2023.
- [27] S. Huang, Z. Jiang, H. Dong, Y. Qiao, P. Gao, and H. Li, “Instruct2act: Mapping multi-modality instructions to robotic actions with large language model,” *arXiv preprint arXiv:2305.11176*, 2023.
- [28] K. Lin, C. Agia, T. Migimatsu, M. Pavone, and J. Bohg, “Text2motion: From natural language instructions to feasible plans,” *arXiv preprint arXiv:2303.12153*, 2023.
- [29] M. Xu, P. Huang, W. Yu, S. Liu, X. Zhang, Y. Niu, T. Zhang, F. Xia, J. Tan, and D. Zhao, “Creative robot tool use with large language models,” *arXiv preprint arXiv:2310.13065*, 2023.
- [30] T. Tsuji, J. Ohkuma, and S. Sakaino, “Dynamic object manipulation considering contact condition of robot with tool,” *IEEE TIE*, vol. 63, no. 3, pp. 1972–1980, 2015.
- [31] H. Wicaksono and C. Sammut, “Relational tool use learning by a robot in a real and simulated world,” in *Proceedings of ACRA*, 2016.
- [32] J. Brawer, M. Qin, and B. Scassellati, “A causal approach to tool affordance learning,” in *IEEE ICIRS*, pp. 8394–8399, 2020.
- [33] N. Saito, K. Kim, S. Murata, T. Ogata, and S. Sugano, “Tool-use model considering tool selection by a robot using deep learning,” in *IEEE ICHR*, pp. 270–276, 2018.
- [34] P. Zech, S. Haller, S. R. Lakani, B. Ridge, E. Ugur, and J. Piater, “Computational models of affordance in robotics: a taxonomy and systematic classification,” *Adaptive Behavior*, vol. 25, no. 5, pp. 235–271, 2017.
- [35] K. P. Tee, J. Li, L. T. P. Chen, K. W. Wan, and G. Ganesh, “Towards emergence of tool use in robots: Automatic tool recognition and use without prior tool learning,” in *IEEE ICRA*, pp. 6439–6446, 2018.
- [36] J. Sinapov and A. Stoytchev, “Detecting the functional similarities between tools using a hierarchical representation of outcomes,” in *IEEE ICDL*, pp. 91–96, 2008.
- [37] S. Forestier and P.-Y. Oudeyer, “Modular active curiosity-driven discovery of tool use,” in *IEEE ICIRS*, pp. 3965–3972, 2016.
- [38] S. Ding, J. Peng, J. Xin, H. Zhang, and Y. Wang, “Task-oriented adaptive position/force control for robotic systems under hybrid constraints,” *IEEE TIE*, 2024.
- [39] H. Ochoa and R. Cortesão, “Impedance control architecture for robotic-assisted mold polishing based on human demonstration,” *IEEE TIE*, vol. 69, no. 4, pp. 3822–3830, 2021.
- [40] M. Selvaggio, A. Garg, F. Ruggiero, G. Oriolo, and B. Siciliano, “Non-prehensile object transportation via model predictive non-sliding manipulation control,” *IEEE Trans. on Control Systems Technology*, 2023.

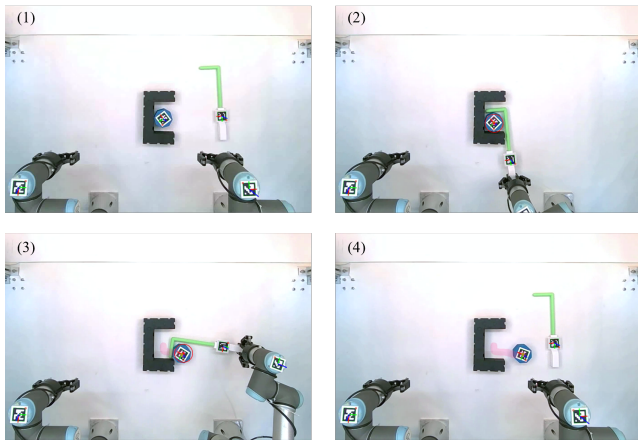


Figure 22: Case 7: (1) Observe the scene; (2) the right arm grasps the hook and approaches the blue block by aligning the top part of the tool to the wall; (3) the blue block is dragging out slowly with the hook being repositioned and rotation-dragging; (4) the blue block out and the hook is returned to its original place.

- [41] M. B. Imtiaz, Y. Qiao, and B. Lee, “Prehensile and non-prehensile robotic pick-and-place of objects in clutter using deep reinforcement learning,” *Sensors*, vol. 23, no. 3, p. 1513, 2023.
- [42] W. Huang, C. Wang, R. Zhang, Y. Li, J. Wu, and L. Fei-Fei, “Voxposer: Composable 3d value maps for robotic manipulation with language models,” *arXiv preprint arXiv:2307.05973*, 2023.
- [43] T. Mar, V. Tikhanoff, G. Metta, and L. Natale, “Multi-model approach based on 3d functional features for tool affordance learning in robotics,” in *IEEE ICHR*, pp. 482–489, 2015.
- [44] D. H. Douglas and T. K. Peucker, “Algorithms for the reduction of the number of points required to represent a digitized line or its caricature,” *Cartographica: the international journal for geographic information and geovisualization*, vol. 10, no. 2, pp. 112–122, 1973.
- [45] A. Fowler and C. Wilson, “Cubic spline: A curve fitting routine,” tech. rep., Union Carbide Corp., Oak Ridge, Tenn. Y-12 Plant, 1966.
- [46] H.-P. Kriegel, P. Kröger, J. Sander, and A. Zimek, “Density-based clustering,” *Wiley interdisciplinary reviews: data mining and knowledge discovery*, vol. 1, no. 3, pp. 231–240, 2011.
- [47] K. Rana, J. Haviland, S. Garg, J. Abou-Chakra, I. Reid, and N. Suenderhauf, “Sayplan: Grounding large language models using 3d scene graphs for scalable robot task planning,” in *7th Annual Conference on Robot Learning*, 2023.
- [48] T. Brown, B. Mann, N. Ryder, M. Subbiah, J. D. Kaplan, P. Dhariwal, A. Neelakantan, P. Shyam, G. Sastry, A. Askell, *et al.*, “Language models are few-shot learners,” *Advances in neural information processing systems*, vol. 33, pp. 1877–1901, 2020.
- [49] M. Pragliola, L. Calatroni, A. Lanza, and F. Sgallari, “On and beyond total variation regularization in imaging: the role of space variance,” *SIAM Review*, vol. 65, no. 3, pp. 601–685, 2023.
- [50] L. Manuelli, W. Gao, P. Florence, and R. Tedrake, “kpam: Keypoint affordances for category-level robotic manipulation,” in *The Int. Symposium of Robotics Research*, pp. 132–157, Springer, 2019.